CORA Cork Open Research Archive
Cartlann Taighde Oscailte Chorcaí

Title	Dual-cavity dual-comb interferometric spectroscopy with incoherent light: Optics and Laser Technology
Authors	Braal, J.;Chandran, S.;Sheehan, R.;Walsh, A.J.;Ruth, A.A.
Publication date	2026-05-01
Original Citation	Braal, J, Chandran, S, Sheehan, R, Walsh, A J & Ruth, A A 2026, 'Dual-cavity dual-comb interferometric spectroscopy with incoherent light : Optics and Laser Technology', Opt Laser Technol, vol. 202, 115393. https://doi.org/10.1016/j.optlastec.2026.115393
Type of publication	Article (peer-reviewed)
Link to publisher's version	https://www.scopus.com/pages/publications/105037463913 - 10.1016/j.optlastec.2026.115393https://www.scopus.com/pages/publications/105037463913?origin=resultslist
Rights	© 2026, the Author(s). Published by Elsevier Ltd. This is an open access article under the CC BY license (http://creativecommons.org/licenses/by/4.0/) - https://creativecommons.org/licenses/by/4.0/
Download date	2026-11-02 18:36:34
Item downloaded from	https://hdl.handle.net/10468/18951

UCC
University College Cork, Ireland
Coláiste na hOllscoile Corcaigh

Optics & Laser Technology 202 (2026) 115393

Contents lists available at ScienceDirect

Optics and Laser Technology

journal homepage: www.elsevier.com/locate/optlastec

Full length article

Dual-cavity dual-comb interferometric spectroscopy with incoherent light

Jarni Braal [a,b], Satheesh Chandran [a,b], Robert Sheehan [a], Anton J. Walsh [b,1], Albert A. Ruth [a,*]

[a] School of Physics & Sustainability Institute, University College Cork, Cork, Ireland
[b] Centre for Advanced Photonics and Process Analysis, Munster Technological University, Cork T12 P928, Ireland

ARTICLE INFO

Keywords:
Cavity-enhanced absorption spectroscopy
Dual-comb interferometry
Trace gas detection
Broadband
Incoherent light
Atmospheric science

ABSTRACT

We show that high-resolution cavity-enhanced dual comb absorption spectroscopy can be performed by creating beat spectra with light transmitted by two high finesse optical cavities of similar lengths, which were neither actively stabilized nor locked to the excitation wavelengths. The incoherent light from a superluminescent light emitting diode (~1535–1560 nm) was spectrally narrowed through filtering (~50 GHz), amplified, and subsequently coupled into two quasi-confocal optical cavities. The light leaking from the two cavities contains all frequencies that belong to the cavities' mode structures, which in the case of confocal cavity geometries resembles in essence a frequency comb. When overlapped and detected as a function of time an interferogram is observed whose Fourier transform yields a regular beat spectrum. The frequencies in the beat spectrum are determined by the difference of the free spectral ranges of the two cavities. The average free spectral range of the cavities determines the spectral resolution of this dual-cavity dual-comb interferometric method. The absolute frequency calibration can either be done through the known position of a target species absorption feature or by beating the comb with an appropriate single mode laser frequency. We demonstrate this approach through measurements of spectra of C_2H_2, CO_2 and H_2O and discuss its applicability, advantages, and limitations.

1. Introduction

Dual-comb (multiheterodyne) spectroscopy (DCS), first demonstrated ca. 20 years ago [1–4], is known as a powerful tool to measure broadband absorption spectra with high resolution. In DCS the frequency scale is established from the interference of two (optical or infrared) *phase coherent* frequency combs with slightly different comb line spacing, which are overlapped on a photodetector. The resulting beat frequencies in the radio frequency (RF) region are determined through a Fourier transformation of the detector signal, and the frequency scale of the two combs can hence be established relative to a frequency calibration point. In the case of octave spanning combs [5] the scale calibration can be linked to a well-defined RF and is hence highly precise in the optical frequency region.

If light from one or both frequency combs is guided through a sample, then the absorption signature of the sample becomes observable in the RF beat spectrum, and high resolution absorption spectra can be obtained [4,6]. By increasing the light-sample interaction path the absorption sensitivity can be improved substantially, for example in open-path applications [7–10]. In laboratory instruments long pathlengths are typically achieved either by sending the light beam through the sample multiple times (in multi-pass reflection cells) [11,12], or by using optically stable cavities typically consisting of two highly reflecting dielectric mirrors [11,13–16]. While in applications with multipass cells there are no constraints on the frequency comb spectrum, for optical cavities in contrast the comb spectra must agree with the eigenmode structures of the cavities. The latter requires either mode matching of the comb frequencies to the mode structures of the cavities [13,14,17] in conjunction with an active locking scheme, or the passive coupling of the combs to the cavity by using an off-axis alignment scheme [18,19]. The latter case is experimentally simpler at the expense of a generally somewhat smaller signal-to-noise ratio.

Here we are suggesting a different approach to measuring cavity-enhanced absorption spectra using the DCS measurement principle involving an incoherent light source. The new approach is making use of two optical near-confocal cavities of slightly different lengths generating axial mode structures with slightly different free spectral ranges (FSRs). The light transmitted by the cavities is recombined and detected on a

* Corresponding author.
E-mail address: a.ruth@ucc.ie (A.A. Ruth).
[1] Passed away: 9 February 2024.

https://doi.org/10.1016/j.optlastec.2026.115393
Received 3 December 2025; Received in revised form 3 April 2026; Accepted 21 April 2026
Available online 1 May 2026
0030-3992/© 2026 The Author(s). Published by Elsevier Ltd. This is an open access article under the CC BY license (http://creativecommons.org/licenses/by/4.0/).

single photo detector of appropriate bandwidth where a time-dependent interference pattern is observed. Observation of the beat pattern becomes possible as the cavities act as a phase filter for the incoherent light. Initial work in this direction was published by Chandler and Strecker in 2012 [20], where a dye laser generating ns pulses with a band-width of ~0.3 cm^{-1} (significant coherence) was used. The experiment was based on the cavity ring-down principle in which the dye laser was tuned to different wavelength ranges and spectral segments had to be concatenated to yield a spectrum. In contrast, in our continuous wave approach we are essentially combining incoherent broadband cavity-enhanced absorption spectroscopy (IBBCEAS) [21,22] with DCS. In IBBCEAS incoherent light is coupled into an optical cavity of high finesse and wavelength selection is carried out after the cavity, where the transmitted light is typically either dispersed with a polychromator and detected with a CCD camera [23], or an interferometric detection scheme (e.g. a Fourier transform spectrometer) is applied [24,25]. A precondition for IBBCEAS is that the FSR of the optical cavity must be much smaller than the spectral resolution of the detection scheme used for the absorption measurement. Under these conditions the mode structure of the cavity becomes unimportant in IBBCEAS even for high finesse near-confocal cavities, because enough light is always transmitted by the cavity in order to be detected by a sensitive photodetector. The method is simple and robust, and highly appropriate for samples with sufficiently broad absorption features in comparison to the spectral resolution, which is the case for many target species and experimental situations in atmospheric trace gas detection. However, if narrow absorption lines are to be detected, e.g. H_2O absorption lines under atmospheric conditions, the limited spectral resolution can lead to non-Lambert-Beer behaviour in the absorption measurement, which needs to be accounted for in the retrieval of absolute extinction coefficients [26,27]. By combining IBBCEAS with DCS this limitation can be overcome, and, depending on the FSR chosen for the cavities used, high spectral resolution can be achieved with high time resolution. We refer to the amalgamation of IBBCEAS and DCS as Dual-Cavity Dual-Comb INterferometry (DC-COIN). It differs considerably from cavity-enhanced dual-comb spectroscopy (CE-DCS), because no frequency comb lasers are actually employed. CE-DCS as an approach to obtain broad high resolution absorption spectra with high time resolution is a very powerful method, which has received significant attention in recent years [14–16,28–36]. However, there are several non-trivial experimental and/or practical challenges in CE-DCS, such as mode matching, laser stability and synchronization, phase noise, cavity dispersion, and frequency shifts for example. Some of which can be alleviated by DC-COIN as will be discussed in this publication.

In Section 2 the experimental setup is outlined, the data retrieval described, and calibration aspects of the method are considered. Experimental absorption results are shown in Section 3 and the approach is validated experimentally based on absorption spectra of H_2O, CO_2, and C_2H_2. Before the work is summarized in Section 5, the advantages and drawbacks of DC-COIN are discussed in Section 4, together with considerations concerning its applicability in practical terms.

2. Experiment

2.1. Overview

A schematic of the experimental setup (DC-COIN) is shown in Fig. 1. Light from a fibre-coupled narrow bandwidth incoherent light source (Section 2.2) was collimated, split into two beams, and coupled into two near-confocal optical cavities of slightly different length (Section 2.3). The light transmitted by the cavities was made to beat inside an optical fibre and detected by a fast (free-space) photodiode (Section 2.4). The Fourier transformed signal of the photo-diode delivers the beat spectrum in the RF region containing the information of the original modes being transmitted. When the frequencies sustained in the cavities coincide

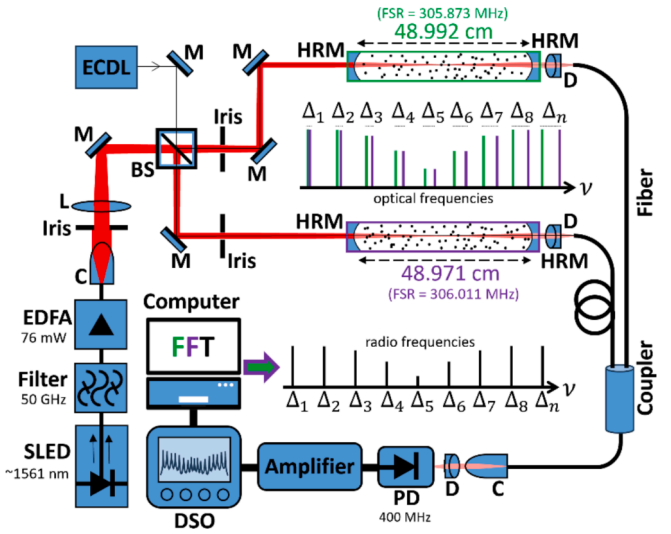


Fig. 1. Schematic of the experimental setup. L: Lens; M: steering Mirror; BS: Beam Splitter cube; HRM: High Reflectivity (R ~ 0.9998) cavity Mirrors; PD: free-space Photo-Diode (bandwidth 400 MHz); SLED: Superluminescent Light Emitting Diode, EDFA: Erbium Doped Fiber Amplifier, gain 30.7 dB, optical output power ~50 mW; ECDL: External Cavity Diode Laser used for absolute wavelength calibration; DSO: Digital Storage Oscilloscope; FFT: Fast Fourier Transformation; C: Collimator (fibre output power ~0.32 μW); D: Doublet lens (Thorlabs AC254-030-C); The filter has a bandwidth of ~50 GHz and is tunable. Fibre: core diameter ~8 μm (single mode).

with an absorption feature of a target species, the beats in the RF spectrum will be diminished (Fig. 1), and absolute extinction coefficients can be retrieved (Section 2.5). The absolute frequency scale needs a calibration point, e.g. through a known absorption line in the spectrum or a laser of known frequency (Section 2.6). It should be noted that the entire setup was merely passively stabilized (see Fig. S1 in the supplementary material), i.e. it is mounted inside a perspex box on a thermally stabilized breadboard, which is resting on a layer of bubble wrap on an ordinary optical bench. No active optical cavity stabilization or locking electronics were employed.

2.2. Light source and beam path

The DC-COIN method hinges on the availability of appropriate light sources. Due to the passive coupling of light to the cavity the optical losses are severe and a high brightness source is therefore required. For this study (and in contrast to [20]) we decided to perform the experiment with an incoherent light source whose emission bandwidth was to be relatively narrow (~50 GHz), but sufficient to cover typical Doppler-broadened ro-vibrational overtone transitions of trace gas species in the near IR. Selecting such a light source was more challenging than anticipated, because typical incoherent light sources, such as continuous wave light emitting diodes (LED), have bandwidths (full width half maximum, FWHM) that are significantly broader than 50 GHz. We used a superluminescent LED (Superlum SLD-761) with an emission spectrum centered at 1561 nm (FWHM ≈ 50 nm; trace (a) in Fig. 2) and at total power of ~8.5 mW. The SLED was temperature controlled at ~20°C and driven with a current of 400 mA. The light from the fiber-coupled SLED was then passed through a narrowband optical filter (Santec OTF-320) to give an optical bandwidth of FWHM ≈ 0.4 nm (~50 GHz at 1561 nm), see trace (b) in Fig. 2. The optical power after passing through the manually tunable filter was 57.5 μW. The light transmitted by the filter was in turn amplified using an erbium doped fibre amplifier (EDFA, JDSU OA 400) with an amplified spontaneous emission noise level of −20 dBm at 1550 nm. When its pump laser is operating at 500 mA and when driven at this current the EDFA has a gain of ~31.2 dB resulting in

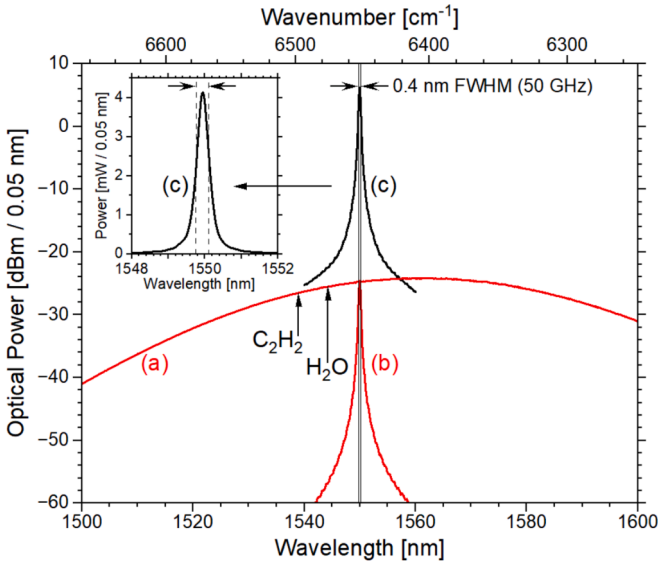


Fig. 2. Spectrum of the incoherent excitation light source on logarithmic and linear power scales. (a) spectrum of the SLED ($P = 8.5$ mW, 400 mA, $T = 20°C$), (b) spectrum of the light after the narrowband filter ($P = 57.4$ μW, FWHM 50 GHz), (c) spectrum of the optical filter output amplified by an EDFA ($P \sim 50$ mW). All components are single mode fibre coupled. For measurements with H_2O and C_2H_2 (see Sections 2.5 and 3.2 respectively) the filter was tuned to the position indicated by the vertical arrows. Inset: Spectrum of the filtered and amplified SLED on a linear power scale.

an output power of ~50 mW (see trace (c) in Fig. 2). The spectra of the SLED (a), the filtered output (b), and the filtered and amplified output (c) were measured with an optical spectrum analyser (OSA, Yokogawa AQ6370D) and are summarized in Fig. 2. While the OSA was calibrated in wavelength but not in absolute photon intensity, all optical powers stated here were measured with an integrating sphere photodiode (Thorlabs S144C).

The SLED, the spectral filter and the amplifier were all single mode fiber coupled (core ~8 μm). The light exiting the fiber was collimated (Thorlabs F260APC-1550) and split (Thorlabs CM1-BS015) 50:50 into two beams which propagated along approximately equal distances to the two stable quasi-confocal cavities (see Fig. 1). The light transmitted by the cavities was again free-space coupled into two single mode fibers, which were brought together into one fiber using a fiber coupler (Thorlabs TN1550R5A1). In this last fiber the transmitted light from the cavities overlapped, causing interference. The light exiting the fiber was again free-space coupled to a detector (Thorlabs APD430C, DC-400 MHz, variable gain).

2.3. Optical cavities

Each of the optical cavities consisted of two dielectric mirrors (cc/pl, diameter 12.7 mm, Layertec GmbH) with a radius of curvature of 50 cm. The mirrors had a nominal reflectivity of $R > 0.9999$ from 1500 to 1610 nm (finesse $> 10^4$). The distance between the mirrors was chosen such that they were close to confocal, with distances of 48.992 cm and 48.971 cm. The corresponding FSRs of the cavities were 305.873 MHz and 306.011 MHz, respectively. For this geometry a "quasi-degeneracy" of transverse modes can be expected and the output from the cavities should exhibit beats with a spacing of ~140 kHz. Over the FWHM of the light source (0.4 nm, Fig. 2) ~163 beats can be expected.

The high reflectivity mirrors were mounted inside two custom-made holders, which also served as gas inlets/outlets for the enclosed cavities. The holders were connected by FEP tubing (diameter 9.5 mm) mounted into standard kinematic mirror mounts inside an optomechanical cage, which was installed on an optical breadboard (see Fig. S1, supplementary material). The whole cavity setup was kept in a perspex enclosure. It should be noted that the cavities were not *actively* stabilized in any way. A passive stabilization was achieved through thermalizing the base of the breadboard to ≈28 °C (i.e. ~5°C over ambient room temperature), and through resting the base plate and enclosure on several layers of 'bubble wrap' on a solid optical bench (L × W × H: 120 cm × 90 cm × 30 cm; *not* vibration isolated). The measures taken to mechanically stabilize the cavity are not necessary per se, but improve the signal-to-noise ratio (SNR) in the data retrieval described in Section 2.5.

2.4. Detection scheme

The combined light signal from both cavities was detected with an avalanche photodiode (Thorlabs APD430C, 400 MHz, not fibre-coupled, variable gain), which was connected to a digital storage oscilloscope (Rohde & Schwarz, RTE1204, 2 GHz, maximum digital acquisition memory size 200 Mpts). The signal was measured with an arbitrary start time ($t = 0$ s) for an integration time of 200 ms in a free running manner. Since the zero-time is arbitrary, the experiment neither requires any synchronization or external trigger, nor feedback loops, locking schemes or active electronic stabilization; it is "free running". Since a broadband light source is used, no scanning is required either, the wavelength range is simply determined by the optical filter (Section 2.2). The waveforms from the oscilloscope were then processed on a computer with a bespoke python procedure which is briefly outlined in the next Section 2.5.

2.5. Data analysis and extinction retrieval

2.5.1. Retrieval of the beat spectrum

While the detector is free running and the cavities are neither actively stabilized nor locked to a particular frequency, the relative frequency positions of the cavities' eigenmodes are subject to thermal drift and mechanical jitter. For sufficiently short time intervals, however, the lengths of the two cavities can be assumed to be constant in good approximation, and light transmitted by both cavities exhibits sufficiently stable mode structures (see schematic panel (A) in Fig. 3). When the light beams transmitted by the cavities are combined, a time-dependent signal (=interferogram) is generated. The typical raw data of such an interferogram is shown in panel (B) in Fig. 3. The adequate processing of this interferogram will yield a final beat spectrum, which is schematically illustrated in the panels of Fig. 3: The measured 200 ms interferogram (Fig. 3(B)), which is measured with a ~1 ns time resolution of the oscilloscope in a typical experiment, is divided into time segments of a duration of ~166.6 μs in such a way that each segment overlaps with 90% of the previous segment (see Fig. 3(C)); more information on the overlap percentage is given in the supplementary material. Adjacent segments therefore have datapoints of ~150 μs in common. This results in ~12,000 time-dependent segments for a 200 ms waveform, which are then individually fast Fourier transformed using Welch window functions. The short duration of the time segments before the FFT guarantees that for each of these time windows the cavity is mechanically stable in good approximation. The resulting segment beat spectra (see panel (D) in Fig. 3) are then evaluated to obtain the overall (final) beat spectrum. The establishment of the ***final beat spectrum*** is achieved in 3 steps:

(1) *Evaluation and selection of the appropriate individual beat spectra*: Not all FFTs of time segments yield qualitatively adequate beat spectra; see panel (D) in Fig. 3. The features of the (frequency-dependent) beat spectra depend on the quality of the interference pattern in each time segment. If an insufficient number of beat notes above 1.8 times the interquartile range of the noise level is observed, or if the expected average frequency spacing between the observed beat notes is not as predicted from the FSRs of the two cavities (within ± 5%), then the corresponding beat

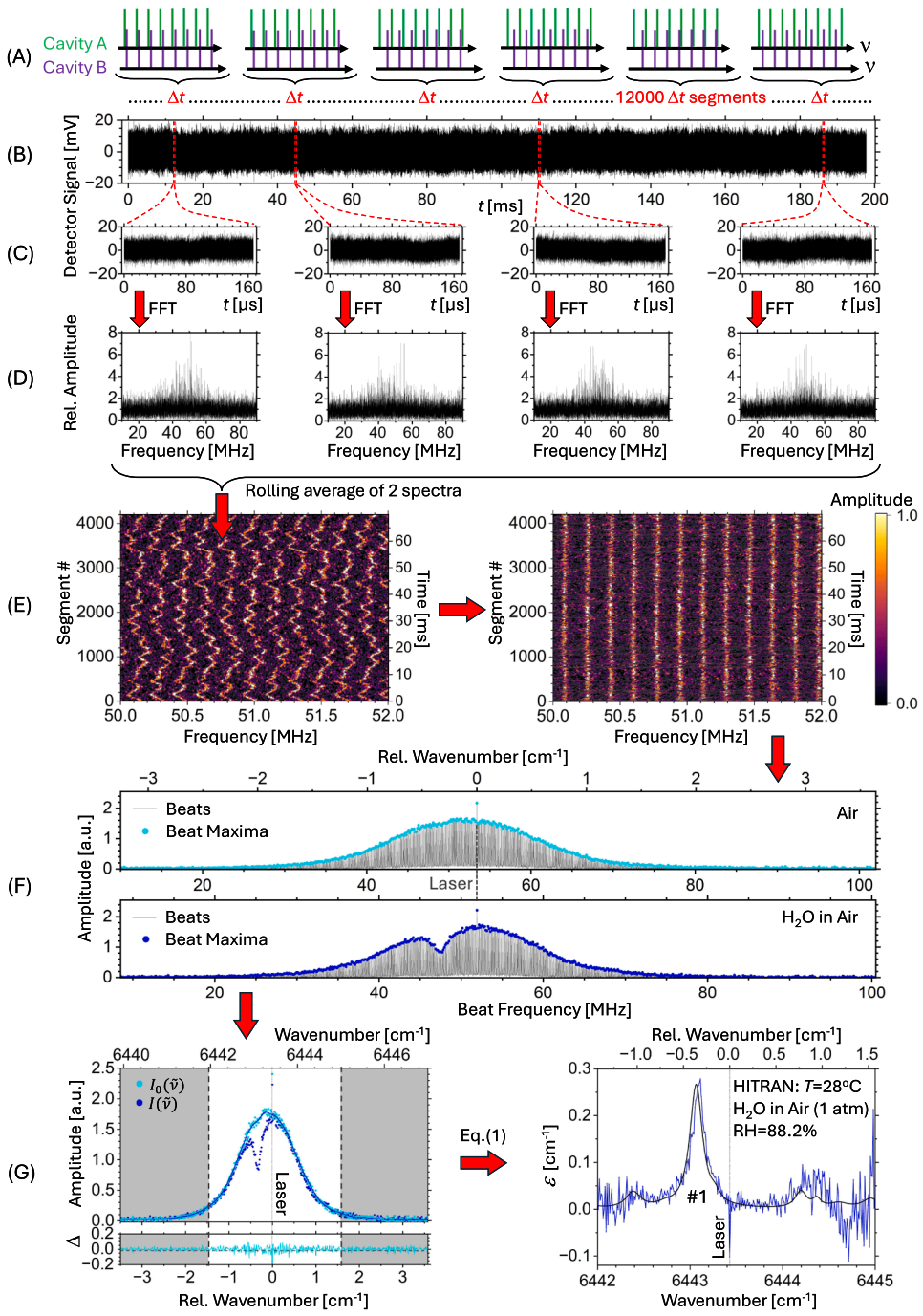


Fig. 3. Visualization of the different steps involved in the extinction retrieval. (A) Schematic representation of the axial modes in the two cavities at different times during data acquisition. (B) Overall time-dependent signal (interference pattern) for a 200 ms acquisition time. (C) Four examples of ~167 μs time segments within the interferogram. (D) Fast Fourier transform (amplitude spectrum) of the four individual segments in panel (C). (E) A section of the amplitude spectra between 50 and 52 MHz (containing ~12 beat notes) in a 3D colour-filled contour plot; left viewgraph (LVG): as recorded (drift and jitter), right viewgraph (RVG): brought into phase (position-corrected). Jitter and drift in this example is smaller than 2.5 times the fundamental beat frequency. (F) Final beat spectra, wavenumber–adjusted according to an external laser line position (vertical dashed line) for measurements without ($I_0(\tilde{\nu})$, upper viewgraph) and with ($I(\tilde{\nu})$, lower viewgraph) a target species (in this case H_2O) in the cavity. Note that wavenumber calibration can be alternatively based on a known absorption line feature of a calibration gas in the mixture instead of an external single mode laser (Section 2.6). (G) LVG: $I_0(\tilde{\nu})$ and $I(\tilde{\nu})$ spectra (light and dark blue dots respectively), 10-point FFT–interpolated $I_0(\tilde{\nu})$ (solid dark blue trace) and residuals (solid dark blue trace). Data in the grey areas are not considered in eq. (1). The small "dent" in I_0 is attributed to water absorption outside the cavity. RVG: Final extinction spectrum calculated from the measurement in panel (F) using eq. (1), solid dark blue line. A simulated HITRAN spectrum [37,38] for RH = 88.2% is represented by the black trace. The small shift between the simulation and the measured extinction spectrum is smaller than the uncertainty of the absolute wavelength calibration of the laser position of 0.08 cm^{-1} (see Section 2.6). Vertical dashed lines indicate the calibration laser position. Assignment #1 stated in Table 2.

spectrum was not included in the evaluation procedure. Another selection criterion is due to the free running of the experiment and is illustrated in the supplementary material (Fig. S2). Typically 6–7% (min ~ 0%, max < 15%) of the individual time segments were discarded in a regular measurement. A rolling

average of 2 time segment beat spectra is then formed, which gives a large set of individual beat spectra as a function of time.

(2) *Phase correction of the individual beat spectra*: Since the measurement is free-running and because the cavity lengths are subject to some mechanical jitter and limited thermal drift, the frequency positions of the beat notes are not constant but vary slightly from beat spectrum to beat spectrum. This is shown in the left viewgraph of panel (E) in Fig. 3. Approximately one third (~4200) of the Fourier transformed segments in a measurement are shown in the frequency range between 50 and 52 MHz (containing ~12 beat notes) in a 3D colour-filled contour plot. The normalized amplitude obtained in the FFT is given by the color palette on the right in panel (E). To bring the beat notes into phase with one another the individual beat spectra are shifted into position (one after another), typically by less than the fundamental beat frequency difference (<170 kHz). Shifts larger than the fundamental beat frequency difference were observed on occasions depending on the general stability of the hardware; all shifts applied were smaller than maximally ~3–4 times the fundamental beat frequency difference (see also Fig. 3(E)).

(3) *Averaging of beat spectra*: Once all individual beat spectra are brought "into phase", they are summed up and the amplitude maxima and their positions in the final beat spectrum are determined (with beat separation in the ~kHz range covering overall -tens of MHz – Fig. 3(F)).

The upper viewgraph in panel (F) in Fig. 3 shows an example of a final beat spectrum measured with dry aerosol-free air in the cavities. Following the DCS measurement principle each beat frequency in the final beat spectrum (in the RF region) can be unambiguously assigned to a relative optical frequency by scaling it with the mean FSR of the cavities; the applicable criteria and a short discussion is given in Section 3.1. The relative optical frequencies are then typically converted to a *relative wavenumber scale* (see upper axis on viewgraphs in Fig. 3(F)), which requires a calibration point within the spectrum in order to be turned into an *absolute wavenumber scale*. Experimental options and further details for this wavenumber calibration are described in Section 2.6.

2.5.2. Retrieval of the extinction spectrum

The retrieval of the extinction spectrum is based on the IBBCEAS approach [21]. The beat maxima as a function of wavenumber constitute the intensity spectrum, $I(\tilde{\nu})$, of the light transmitted by the two cavities. In order to obtain the final extinction spectrum of a gaseous sample in the cavities, $\varepsilon(\tilde{\nu})$, the following quantities are required; (i) a "zero measurement" without a sample, $I_0(\tilde{\nu})$, (ii) the mean of the cavity lengths, d, and (iii) the reflectivity, $R(\tilde{\nu})$, of the mirrors (discussed in Section 3.1) [21,23]:

$$\varepsilon(\tilde{\nu}) = \frac{(1 - R(\tilde{\nu}))}{d}\left(\frac{I_0(\tilde{\nu})}{I(\tilde{\nu})} - 1\right) \quad (1)$$

The spectral resolution, with which $\varepsilon(\tilde{\nu})$ can be measured, depends to the mean FSR of the two cavities. Since the spectral resolution of the approach is high, the most straightforward way of obtaining $I_0(\tilde{\nu})$ is by simply interpolating the intensity spectrum $I(\tilde{\nu})$ in between apparent absorption features (see Ref. [25]). This is possible if the spectral region is wide enough, and a clear and sufficiently smooth outline of the extinction-free part of the spectrum is discernible. Alternatively, if the spectrum does not contain sufficient spectral stretches free of optical losses (absorption & scattering), then two measurements of intensity spectra, $I(\tilde{\nu})$ and $I_0(\tilde{\nu})$, with and without the target sample are required as illustrated in Fig. 3. An absolute wavenumber scale is required to line up the two spectra $I(\tilde{\nu})$ and $I_0(\tilde{\nu})$ (see next Section 2.6).

The upper viewgraph in panel (F) of Fig. 3 shows a measurement without a sample (dry aerosol-free air, 1 atm), while the lower viewgraph shows a measurement with humidified air as a sample gas (RH = 88.3%, T = 28°C, 1 atm). The data in the upper viewgraph in panel (F) constitute $I_0(\tilde{\nu})$, while those in the lower viewgraph of the same panel correspond to $I(\tilde{\nu})$. In the left viewgraph of panel (G) in Fig. 3 $I(\tilde{\nu})$ and $I_0(\tilde{\nu})$ are shown again (light and dark blue dots). To reduce noise $I_0(\tilde{\nu})$ is adequately smoothed with an FFT filter (=dark blue solid line) as indicated by the absolute residuals at the bottom of this viewgraph. Using the interpolated $I_0(\tilde{\nu})$ as well as $I(\tilde{\nu})$ in eq. (1) finally leads to the extinction spectrum, $\varepsilon(\tilde{\nu})$, shown in the right viewgraph of panel (G) of Fig. 3 (dark blue line). This water absorption spectrum has been simulated with data from the HITRAN database [37,38], shown as a solid black line in the spectrum. The assignment of the line is stated in Table 2.

2.6. Absolute wavenumber calibration

There are two ways to obtain a wavenumber calibration point in the spectrum, which is not only essential from a spectroscopic point of view for assignments of absorption features and identification of target species, but also to align $I(\tilde{\nu})$ and $I_0(\tilde{\nu})$ in the retrieval process of the extinction as seen in the previous section:

(A) *Using a laser*: A stable single mode "calibration laser" of known frequency can be coupled into one or indeed both of the cavities (see ECDL in Fig. 1). The laser is then sufficiently slowly scanned over a small frequency range of the order of the cavities' FSR. When the laser comes into resonance with a cavity mode in one of the cavities the acquisition of the time-dependent interferogram is triggered. The single mode laser frequency will then occur as strong beat in the final beat spectrum and its position constitutes the frequency calibration point. This approach was chosen in this work. The laser interference can be seen in the panels (F) and (G) of Fig. 3 (marked with vertical dashed lines) and was chosen as the zero point for the relative wavenumber scale of the final beat spectra. In this work the wavenumber position of the laser was determined using a Fourier Transform Spectrometer (Bruker Vertex 80), whose resolution is 0.08 cm^{-1} (=2.4 GHz). The absolute wavenumber scale of the spectrometer was calibrated using a measured water spectrum and the corresponding wavenumber positions from HITRAN [37]. Thus the uncertainty of the absolute spectral position of the laser equals the resolution of the FTS and we consider this to be the uncertainty in the absolute wavenumber scale.

(B) *Using a calibration gas*: Alternatively, a wavenumber calibration point can also be provided by at least one known absorption line within the wavenumber region considered. If a calibration gas (e.g. CO_2) is present during the measurement of $I(\tilde{\nu})$ *and* $I_0(\tilde{\nu})$, then the spectra can be aligned for the extinction coefficient retrieval on an absolute wavenumber scale based on the known calibration gas absorption position(s). As mentioned before, in cases where the calibration gas absorption lines are narrow and the overall wavenumber range is wide, interpolation between the gas lines is also possible to obtain an I_0 spectrum [25]. A measurement is then sufficient to retrieve the extinction spectrum, which, if it contains known absorption lines can be used for wavenumber calibration.

2.7. Sample gases and flow settings

The sample gases in proof-of-concept measurements here were either carbon dioxide, CO_2, from a cylinder (Irish Oxygen, >99.9%) or acetylene, C_2H_2, from a welding cylinder (purity >95%). Either gas was mixed into 'dry' (dewpoint –60°C) and 'aerosol-free' (1 μm particle filter) compressed air. One measurement was taken with humidified air at RH ~88% (Fig. 3(G)). A mass flow controller (Alicat, MFC-50SCCM-D/5M) was used to set the volumetric flow rate to 20 sccm. The gas inlet line was split into two equal lengths (ca. 20 cm) of FEP Teflon tubing (diameter 1/8 in., OD), which were each connected with one of the optical cavities (not shown in Fig. 1, cf. Section 2.3 and Fig. S1). The cavities were flushed with dry and aerosol-filtered compressed air

between measurements. All experiments were run at a pressure of $P \sim 1$ atm and temperature of $T \sim 28°C$.

3. Results

3.1. Fundamental cavity modes

The beats of the fundamental axial cavity modes in each of the two cavities can also be observed in the FFT of the overall (200 ms) time-dependent detector signal. The beat frequencies correspond to the FSRs of each of the cavities. Fig. 4 shows the fundamental cavity modes taken during the H_2O measurement shown in Fig. 3(F) and (G). They are located around 306 MHz and are based on the cavity configuration outlined in Section 2 (cf. Fig. 1). From the modes' FWHM and FSR the cavities' average finesse and hence reflectivity in eq. (1) can be established, which enables the measurement of absolute extinction coefficients. Since the evaluation of the reflectivity is an inherent part of dual-cavity dual-comb interferometric spectroscopy (similar to conventional pulsed cavity ring-down spectroscopy), the sample's absolute extinction signal does not require calibration with a known amount of sample of known absorption or scattering cross-section, like in the case of IBBCEAS [21,23].

Under ideal conditions a mode spectrum should have a Lorentzian shape and indeed, fitting Lorentzian profiles to the modes yielded reasonable results (see supplementary material, Fig. S3). However, the maxima of the mode profiles could in many cases not be modelled satisfactorily by a Lorentzian, which impinges on the retrieval of the mode widths and leads to a small but systematic underestimate of the reflectivity. Therefore we established the FWHM from the mode spectra directly by smoothing the data with a 10-point Fourier transform filter as shown in Fig. 4. This approach yielded fundamental mode frequencies of 305.873 and 306.011 MHz, and mode widths (FWHM) of $\delta\nu \sim 20.2$ and 22.3 kHz (Table 1). From the mode widths and FSRs the finesse and reflectivity were established for each cavity (Table 1), and subsequently averaged. In this way a mirror reflectivity of $R = 0.99978 \pm 0.00002$ was found for the experiment shown in Fig. 3(F) and (G), which is based on a mean finesse of 14420. Extra information on the general uncertainties are given in the supplementary material (Figs. S3 and S4).

3.2. Absorption spectrum of carbon dioxide and acetylene

3.2.1. Carbon dioxide

Fig. 5 shows the final beat spectra ($I_0(\tilde{\nu})$ and $I(\tilde{\nu})$ in panels (A) to (C)) and the resulting extinction spectrum ($\varepsilon(\tilde{\nu})$ in panel (D)) for a measurement of carbon dioxide (CO_2) in dry compressed air around ~6495 cm^{-1}. For these spectra the 50 GHz filter (see Fig. 1) was tuned by ~50 cm^{-1} to higher wavenumbers within the emission spectrum of the SLED in comparison to the water spectrum shown in Fig. 3. In Fig. 5(A) the final beat spectrum (fine grey lines) for N_2 (1 atm) in the cavities is shown together with the highlighted maxima of the beats, shown as light blue dots. The beat maxima were interpolated with a 12-point FFT filter shown as a solid blue trace in panel (A). The latter constitutes $I_0(\tilde{\nu})$ in eq. (1). The absolute residuals, Δ, of this interpolation is shown in panel (B) of Fig. 5. The beat spectrum in panel (A) was measured immediately before the final beat spectrum obtained with CO_2/air mixture in the cavities shown in Fig. 5(C). The beat maxima (blue dots) represent $I(\tilde{\nu})$ in eq. (1). In both beat spectra there is one strongly increased beat line indicating the spectral position of the external cavity diode laser (cf. Fig. 1), whose position at 6495.48 cm^{-1} was taken as a wavenumber reference point for the extinction spectrum (solid blue line) shown in Fig. 5(D). To calculate the extinction spectrum with eq. (1) the shaded grey regions in the beat spectra in panels (A) to (C) were left out because the light source intensity was too small in those regions to deliver meaningful results. Note that the start and end points of the frequency regimes in both beat spectra are different (panel (A): ~12–72 MHz, panel (C) ~32–92 MHz). This is due to the fact that the acquisition is free running and not time synchronized. The width of ~60 MHz is however the same in both beat spectra. The CO_2 extinction spectrum was modelled as per the HITRAN database [37] yielding a mixing ratio of CO_2 of ~5% by volume [38]. The relevant absorption lines in the spectral region of interest are labelled in the Fig. 5(D) and the corresponding assignments are listed in Table 2 for information. It should be noted that the black solid line in Fig. 5(D) constitutes a simulation based on the measurement conditions and not a fit to the spectrum.

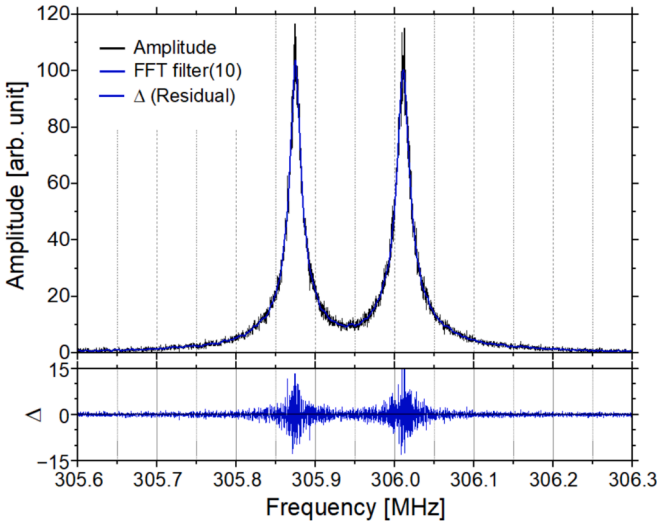


Fig. 4. Spectrum of the fundamental axial modes (black trace) of the two cavities as obtained from a fast Fourier transform of 200 ms of the detector signal. The two quasi-Lorentzian profiles were interpolated with a 10-point FFT filter to retrieve the parameters shown in Table 1. The lower panel shows the absolute (unweighted) residuals concerning the interpolated data (see also Figs. S3 and S4, suppl. material).

Table 1
Parameters retrieved from the fundamental axial modes of the two cavities for the measurement shown in Fig. 3, panels (F) and (G). Errors are based on the evaluation of 26 different measurements of fundamental modes (see supplementary material, Fig. S4).

Cavity	Long cavity (green in Fig. 1)	Short cavity (purple in Fig. 1)
Length, *d* [mm]	489.924 ± 0.002	489.705 ± 0.002
FSR [MHz]	305.873 ± 0.001	306.011 ± 0.001
Amplitude [arb. unit]	104 ± 2	101 ± 2
Fundamental FWHM, δν [kHz]	20.24 ± 0.55	22.29 ± 0.74
Finesse, *F*	15110 ± 450	13730 ± 480
Reflectivity, *R*	0.99979(2)	0.99977(1)

3.2.2. Acetylene

Fig. 6 shows the final beat spectra ($I_0(\tilde{\nu})$ and $I(\tilde{\nu})$ in panels (A) to (C)) and the resulting extinction spectrum ($\varepsilon(\tilde{\nu})$ in panel (D)) for a measurement of acetylene (C_2H_2) in dry compressed air in the region between 6493 and 6497 cm^{-1}. The figure is constructed in the same way as Fig. 5 and the color code as well as the meaning of symbols and traces are analogous to those in Fig. 5. The C_2H_2 extinction spectrum was modelled as per the HITRAN database [37] yielding a mixing ratio of C_2H_2 of ~0.4% by volume [38]. The relevant C_2H_2 absorption lines in the spectral region of interest are labelled in Fig. 6(D), and the corresponding assignments are listed in Table 2. Interestingly, the spectrum of acetylene features a very weak transition centred at 6495.1(3) cm^{-1}, which can indeed be assigned to the $H^{12}C^{13}CH$ isotopologue of acetylene. We note that the feature coincides with the nearby CO_2 line at 6495.0(7) cm^{-1} in Fig. 5. However, in the acetylene measurement (Fig. 6) dry compressed air containing the natural amount of CO_2 was

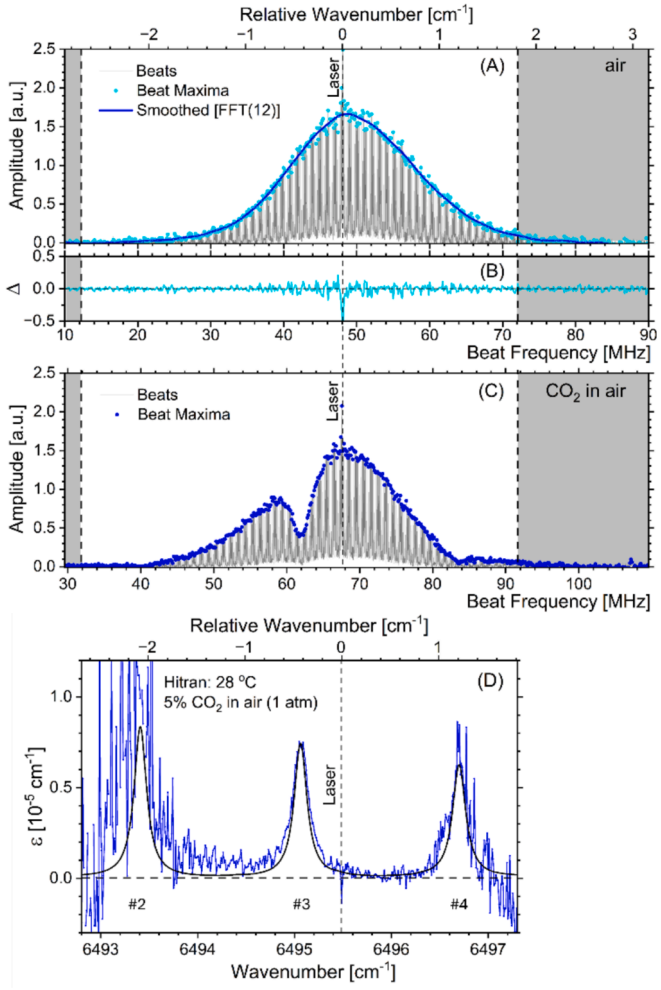


Fig. 5. (A): Final beat spectrum (grey trace), beat line maxima (light blue dots) and FFT interpolated beat spectrum, $I_0(\tilde{\nu})$ (solid blue line) for N_2 (~1 atm) in the cavities. (B): Absolute residuals of the interpolated trace and the beat maxima. (C): Final beat spectrum (grey trace), beat line maxima, $I(\tilde{\nu})$ (blue dots) for 5% of CO_2 in dry compressed air (~1 atm) in the cavities. The spectrum in panel (C) was measured immediately after the spectrum in panel (A). (D): Extinction spectrum (blue trace) calculated with eq. (1) for CO_2 together with a modelled spectrum according to the HITRAN [37] database. Prominent lines with assignments as per [37] are listed in Table 2. The wavenumber axis was calibrated using the beat position of the external cavity diode laser (see Fig. 1).

used for the measurements of $I_0(\tilde{\nu})$ and $I(\tilde{\nu})$, as opposed to measurement with carbon dioxide (Fig. 5), where N_2 was used as zeroing gas. Thus, any CO_2 feature in the acetylene spectrum in Fig. 6 is accounted for by having the same amount of CO_2 in the I_0 and I measurements. Hence the small feature at 6495.1(3) cm^{-1} is indeed based on a transition in $H^{12}C^{13}CH$ isotopologue.

The resolution of the setup of ~300 MHz is well sufficient to resolve the absorption lines absorption lines of H_2O, CO_2 and C_2H_2, which are all subject to collisional and Doppler broadening for the given measurement conditions yielding a typical FWHM of roughly ~0.15 cm^{-1}. It is noteworthy that even in regions of the spectrum where the intensity of the light source is approaching the noise level, absorption features can still be clearly recognized (see Fig. 5(D)).

3.3. Detection limits

The SLED emission spectrum (Section 2.2) was modelled with a Gaussian profile, and the 2σ wavenumber range of ca. 2.6 cm^{-1}, where

Table 2
Spectroscopic assignment of absorption features in Figs. 3, 5, and 6 from Ref. [37]. $\tilde{\nu}$: center (vacuum-) wavenumber, the last digit in brackets indicates the current laser position uncertainty of 0.08 cm^{-1} (absolute uncertainty), the resolution of the measurement is ~300 MHz (≈10^{-2} cm^{-1}). S: line strength multiplied by isotopologue abundance. Assignment: Vibrational and (rotational) quantum numbers and labels for the upper and lower state of a transition [37].

Molecule Figure, label	$\tilde{\nu}$ [cm^{-1}]	S [cm/molecule]	Assignment Upper state		Lower state	
H_2O						
Fig. 3(G), #1	6443.0 (9)	8.07×10^{-25}	0 2 1 (7 1 7)		0 0 0 (8 3 6)	
CO_2						
Fig. 5(D), #2	6493.4 (2)	1.70×10^{-24}	3 0 0 11		0 0 0 01	
Fig. 5(D), #3	6495.0 (7)	1.55×10^{-24}	3 0 0 11		0 0 0 01	
Fig. 5(D), #4	6496.7 (1)	1.34×10^{-24}	3 0 0 11		0 0 0 01	
HC_2H (97.7%)						
Fig. 6(D), #5	6494.0 (3)	1.88×10^{-22}	101 0 1 0 1	g	000 0 1 0 1	u
Fig. 6(D), #6	6494.5 (1)	4.30×10^{-22}	101 1 0 1 0	u	000 1 0 1 0	g
Fig. 6(D), #7	6494.6 (1)	1.44×10^{-22}	101 1 0 1 0	u	000 1 0 1 0	g
Fig. 6(D), #8	6495.9 (1)	22.14×10^{-22}	101 0 0 0 0 +	u	000 0 0 0 0 +	g
$H^{12}C^{13}CH$ (2.2%)						
Fig. 6(D), #9	6495.1 (3)	0.64×10^{-22}	101 0 0 0 0 +		000 0 0 0 0 +	

sufficient emission power was present, was used to evaluate the minimum detectable extinction coefficient ε_{min} and noise equivalent absorption (NEA). ε_{min} was evaluated based on the 3σ extinction level of the noise in this wavenumber range for five I_0 measurements (without sample), and subsequently averaged. The measurements were chosen from a set of I_0 data that were taken at different days before different CO_2, C_2H_2 and H_2O measurements; i.e. for most measurements the setup and ambient conditions varied somewhat due to e.g. cavity realignments or laser tuning. The I_0 data were hence representative. The laser signal was in all cases ignored in the calculation of the standard deviation. With this approach ε_{min} (3σ) was found to be 7.05×10^{-7} cm^{-1} for the sample-free (air-filled) cavity for a 200 ms integration time (bandwidth, $BW = 5$ Hz). The corresponding noise equivalent absorption is therefore, $NEA = \varepsilon_{min} / \sqrt{BW} = 3.15 \times 10^{-7}$ cm^{-1} $Hz^{-1/2}$ [39]. This translates into 3σ detection limits for CO_2, C_2H_2, and H_2O in air at 1 atm in the two spectral regions shown of ~ 3.8 ppTv, ~1.8 ppmv and ~ 6.25 ppTv, respectively. Note that for this estimate a mean reflectivity value of $R = 0.99978$ was assumed.

To assess the stability of the setup an Allan deviation analysis was performed [40]. Due to the storage limitation of the digital oscilloscope used for the data acquisition (see Section 2), the longest possible acquisition time was 200 ms. Therefore more than 700 subsequent "200 ms measurements" with only air in the cavities (no target gas) were concatenated to yield a total Allan deviation time base of ~70 s (see Fig. 7). Due to the long duty cycle of ~3 min per measurement the total duration of this exercise was >35 hr. The double logarithmic graph in Fig. 7 shows the mean Allan variance as a function of integration time which follows in good approximation the expected slope of –0.5. It illustrates the stability of the setup well in excess of integration times of 10 s despite the fact that the actual duration to establish the data for Fig. 7 was significantly longer than the sum of concatenated acquisition times. The performance of the setup therefore does not seem to be

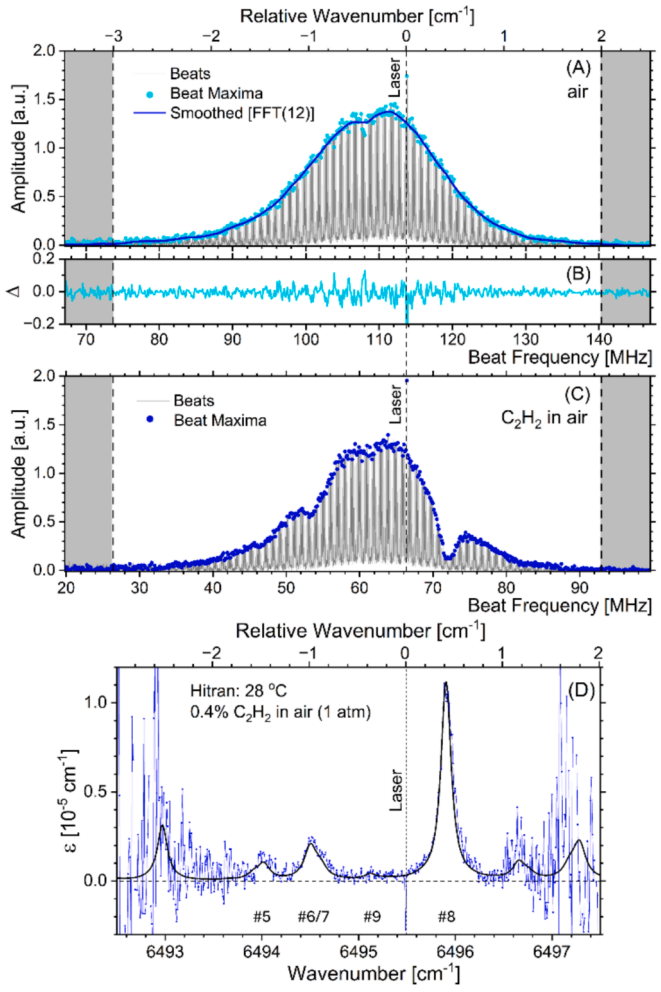


Fig. 6. (A): Final beat spectrum (grey trace), beat line maxima (light blue dots) and FFT interpolated beat spectrum, $I_0(\tilde{\nu})$ (solid blue line) for dry compressed air (~1 atm) in the cavities. (B): Absolute residuals of the interpolated trace and the beat maxima. (C): Final beat spectrum (grey trace), beat line maxima, $I(\tilde{\nu})$ (blue dots) for C_2H_2 in dry compressed air (~1 atm) in the cavities. The spectrum in panel (C) was measured immediately after the spectrum in panel (A). (D): Extinction spectrum (blue trace) calculated with eq. (1) for 0.4% of C_2H_2 together with a modelled spectrum according to the HITRAN [37] database. Prominent lines with assignments as per [37] are listed in Table 2. The wavenumber axis was calibrated using the beat position of the external cavity diode laser (see Fig. 1).

strongly affected by the continued restarting of the acquisition cycle.

4. Discussion

4.1. Applicability of dual-cavity dual-comb interferometric spectroscopy

The DC-COIN approach is different in that incoherent light is used to generate a response of an optically stable cavity; the corresponding *transfer function* simply constitutes a "frequency comb". The transfer functions of the cavities depend on their geometry, i.e. the distance, d, between the two cavity mirrors and the mirrors' radii of curvature, r_{ci}. The geometry is commonly described by the geometry parameters $g_i = 1 - (d / r_{ci})$; i = 1,2. For dual comb spectroscopy the optimum cavity geometry is quasi-confocal, for which $g_i \approx 0$ (i.e. $d \approx r_{ci}$). For the confocal geometry the cavity's transverse modes are virtually all degenerate and the transfer function corresponds to a mode structure that is almost entirely based on the axial modes of the cavity [41]. The corresponding transfer function constitutes a comb-like structure, where the separation of the comb lines is given by the FSR of the cavity. In order to perform dual-comb spectroscopy two cavities of slightly different lengths are being used; i.e. one cavity has a base length, d_0, and the second cavity has a length of $d_0 + \Delta d$. The length difference, Δd, causes the cavities to have slightly different FSRs. When the light from the cavities is overlapped a beat spectrum is observed with frequency spacings

$$\Delta = \frac{c}{2n}\left(\frac{1}{d_0} - \frac{1}{d_0 + \Delta d}\right), \tag{2}$$

which is the difference between the two FSRs, if dispersion is ignored (in eq. (2) n = refractive index of the medium in the cavity, c = speed of light). In dual-comb spectroscopy unambiguous mapping of the beat notes in the RF region to the optical frequencies causing the beating can be made up to a frequency spacing of $\Delta_{imax} = i_{max} \times \Delta < FSR/2$ (see green and purple schematic modes in Fig. 1 and panel (A) in Fig. 3). i_{max} is the maximum number of beat notes that can be unambiguously assigned to a frequency in the optical region. The corresponding maximum usable frequency range that can be addressed without aliasing (for spectroscopic purposes) is $\Delta\nu_{max} = i_{max} \times FSR$ accordingly. Both of these experimentally important parameters, i_{max} and $\Delta\nu_{max}$, depend on the base length, d_0 and cavity length difference Δd. Visualizations for typical cavity base lengths and length differences are shown in Fig. 8 panels (a) and (b), respectively.

The black dots in Fig. 8 represent the dual-cavity geometries used in this publication, where the maximum achievable number of beat notes is $i_{max} = 790$ yielding a maximum frequency range of $\Delta\nu_{max} = 240$ GHz. However, since our filter has only a FWHM of ~50 GHz (Fig. 2) only approximately 164 beat notes were observed. Thus, our theoretically achievable frequency range could in principle be almost 3–4 times larger (i.e. ≈8 cm^{-1}) with a different filter.

In practice the axial modes of the cavities are not infinitely narrow and the modes' finite FWHM, which depend on the cavity mirrors' reflectivities, can in principle hamper the unambiguous assignment of beat notes to optical frequencies. This however becomes only relevant for "low" reflectivities, R, in the case of cavities with low finesse, F. The width of a cavity mode, $\delta\nu$, is given by

$$\delta\nu = \frac{FSR}{F} = \frac{c}{2nd_0}\frac{(1-R)}{\pi\sqrt{R}}, \tag{3}$$

where F and R are the finesse and geometric mean $R = \sqrt{R_1 R_2}$ of the reflectivities of the cavity mirrors, respectively. To find a criterion for when the mode width affects the dual-comb spectroscopy principle one can compare the mode width, $\delta\nu$, with the frequency spacing in the RF beat spectrum, Δ. If the spacing is a minimum factor of K times larger than the mode width,

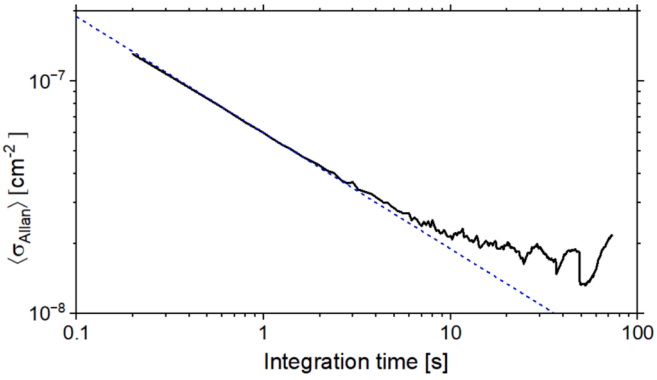


Fig. 7. Solid black line: Mean Allan variance $\langle\sigma_{Allan}\rangle$ of the absorption coefficient as a function of integration time. For this measurement more than ~700 time-dependent acquisitions of 200 ms each were concatenated in a measurement without target species. Dashed blue line: Trace proportional to the expected $t^{-1/2}$ behaviour.

$$K\delta\nu < \Delta, \tag{4}$$

then the dual-comb spectroscopy principle is not affected by the finite mode width anymore. Assuming a quasi-Lorentzian mode profile an initial assumption of $K = 3$ appears to be meaningful corresponding to a 3σ-criterion. However, the linewidths of the beat notes in the RF spectrum (Δ) are not necessarily equivalent to the linewidths of an individual cavity modes (δν). Indeed when comparing the FWHM in the beat spectrum (~29 kHz) with that of the fundamental modes (~21 kHz, Fig. 4) a ratio of ~1.4 was found. The original 3σ-criterion was thus conservatively revised by a ratio of 1.5 to yield $K = 4.5$. K depends on the reflectivity and hence finesse of the cavity and also on the dual cavity parameters d_0 and Δd. Using Eqs. (2)–(4) one obtains:

$$K = F\frac{\Delta d}{d_0} > 4.5. \tag{5}$$

The criterion in Eq. (5) for experimentally viable dual-cavity types (based on F, d_0, and Δd) is graphically illustrated in Fig. 9. Factor K is plotted as a function of the base cavity length, d_0, and the cavity length difference, Δd, for five different finesses, represented through reflectivities between $R = 0.99$ and $R = 0.99999$. Based on criterion in eq. (5) the dual-cavity setups that are represented through parameters above the $K = 4.5$ plane (grey) in Fig. 9 exhibit viable geometries for dual-cavity dual-comb interferometric (DC-COIN) spectroscopy. It is notable that for high finesse cavities ($R = 0.99999$) virtually all dual-cavity geometries fulfil the criterion in eq. (5), even for very small cavity length differences, and base lengths of 1000 mm, because the mode widths become negligibly small. Fig. 9 also shows that the parameters used in this publication are in the viable regime (see caption).

Finally, it should be noted that using a pulsed light source is also possible [20] as long as the pulse duration times the speed of light is larger than the cavity length, so that a mode structure of the cavity can be observed. If the spatial light pulse length is shorter than the cavity length beats in the combined transmission signal cannot be observed.

4.2. Dual-cavity dual-comb interferometry in comparison to CE-DCS and IBBCEAS

DCS is a compelling spectroscopic methodology with numerous superior features [42,43] in comparison to traditional approaches like Fourier transform spectroscopy. Depending on the concrete experimental realization DCS can provide ultimately high spectral resolution [29,44,45] and in many cases (in DCS with mode-locked lasers) absolute frequency calibration is either straightforward or inherently embedded in the experimental approach. These advantages also transfer to experiments where DCS is combined with absorption cavities to improve the overall sensitivity of the setup. However, the use of frequency comb lasers in the context of cavity enhancement introduces several experimental complexities that are related to the required (perfect) mode matching between the two comb sources and the cavity modes. A mismatch can reduce the overall enhancement and accuracy of the measurements. In CE-DCS the two frequency comb lasers ideally need to be fully synchronized and have stable coherence over the observation time. Frequency fluctuations or drift between the combs can lead to uncertainties in the spectral measurements. In some cases they can be compensated through post-processing and specific reference or data reduction schemes in dual comb systems [46–48]. Fluctuations in the relative phase between the frequency combs can introduce noise in the spectral data. E.g. chromatic dispersion can cause a frequency-dependent phase shift between the combs and the cavity modes, which may potentially result in a non-uniform enhancement of the spectral lines. CE-DCS hence relies on robust locking schemes to overcome these challenges. In recent years more and more of these challenges have been overcome and there has been an increasing number of publications on CE-DCS, all of which use phase-coherent frequency combs and locking schemes to match comb lines actively to the cavity modes to stabilize the setup (see also Section 1) [14–16,28,29,31–36,49].

In contrast to CE-DCS, DC-COIN does not require two (potentially expensive) frequency comb lasers. Even though this introduces drawbacks such as optical power limitations or the absolute wavelength calibration issue mentioned above, the omission of the two frequency comb lasers in DC-COIN essentially eliminates several critical experimental challenges. Especially the locking and matching of the comb lines to the cavity modes for given experimental conditions, is essentially not of concern in DC-COIN. The passive coupling of broadband incoherent light to the cavities guarantees the resonance with the cavity modes, however, at the expense of signal strength! Drift and jitter of the cavities can be dealt with through appropriate data processing as outlined in Section 2.

Especially in view of dispersion-based frequency-dependent phase shifts, caused by the cavity mirrors and/or sample gas, DC-COIN may

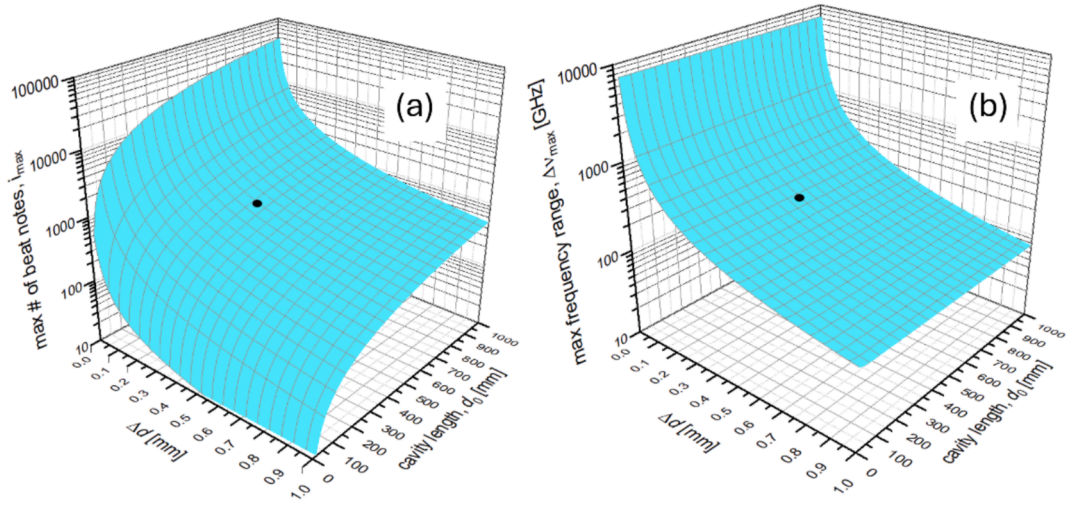


Fig. 8. (a) Visualization of the maximum number of usable beat notes for a given dual-cavity setup as a function of the base cavity length, d_0, and the dual-cavity length difference, Δd. **(b)** Visualization of the maximum frequency range (in [GHz]) that can in principle be achieved without ambiguity in the frequency assignment for spectroscopic purposes for typical cavity lengths, d_0, and the dual-cavity length difference, Δd. For viewgraphs (a) and (b) it is assumed that modes of each cavity are essentially delta function (i.e. they have insignificant FWHM). The black dots represent the cavity parameters of the setup used in this publication, i.e. $d_0 = 498.31$ mm and $\Delta d = 0.32$ mm.

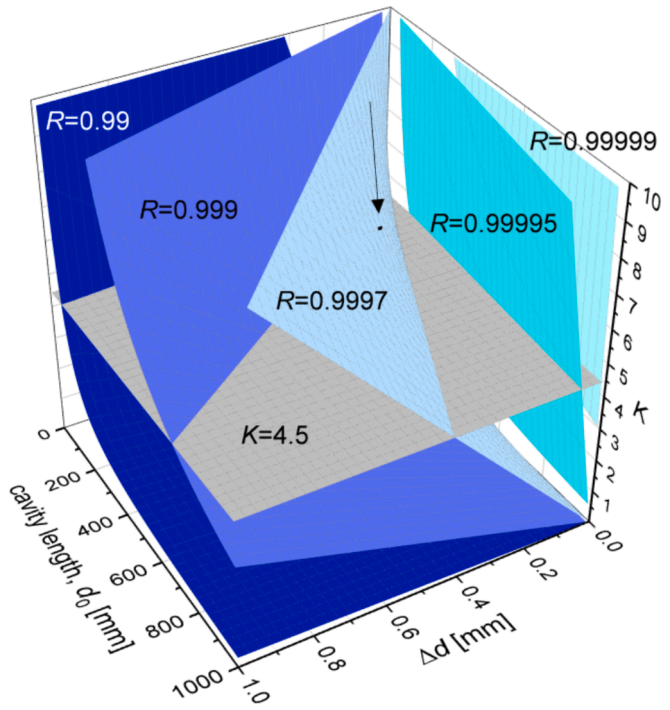


Fig. 9. Graphical visualization of the criterion in eq. (5): factor K as a function of typical base cavity lengths, d_0, cavity length difference, Δd, for five different finesses, represented through reflectivities between $R = 0.99$ and $R = 0.99999$; see the five differently shaded blue surfaces. Based on criterion in eq. (5) the dual-cavity setups that are represented through parameters above the $K = 4.5$ plane (grey) exhibit viable geometries for dual-cavity dual-comb spectroscopy. The arrow points at a black dot which represents the cavity parameters of the setup used in this publication at ~1550 nm; $d_0 = 498.31$ mm, $\Delta d = 0.32$ mm, $R = 0.9997$.

help to resolve some of the issues involved. If a large spectral range is addressed (e.g. of the order of the high reflectivity spectral range of the mirrors), then temperature, pressure, and humidity effects can lead to frequency shifts due to dispersion, which may cause experimental challenges in CE-DCS [45,50].

In high finesse cavities ($>10^4$) with a fully locked optical frequency comb to the cavity, the linewidth of the combs is narrowed down to the fraction of the linewidth of the cavity mode well below kHz. If in this case a large spectral range is addressed, the transmitted intensities will be affected due to the dispersive shift of the cavity resonance, which impinges on the overlap between the narrow comb modes and cavity modes. In other words significant dispersion limit the achievable spectral bandwidth for CE-DCS.

We anticipate that these difficulties should not be prominent with DC-COIN. While the current study only deals with a relatively small spectral region of a few wavenumbers, where chromatic dispersion-related difficulties are negligible in any case, DC-COIN setups are conceivable where a much larger spectral region can be addressed by using a significantly smaller difference of the two cavity lengths than in the present. In these cases both cavities are typically exposed to the same environmental conditions (temperature, pressure, humidity), and therefore the dispersive effects can also be assumed to be approximately equal. Since both cavities essentially act as passive filters of a broadband light source, obtaining a beat spectrum should in principle not be affected by these external influences in DC-COIN. Of course the chromatic dispersion of the setup is not eliminated per se. Thus the scaling of the wavenumber axis can in principle still be affected if a wide spectral range is addressed. However, based on the frequency dependence of the refractive index in air, and on observed typical dispersive shifts in mirrors and samples in the IR [45,50], the uncertainty of the wavenumber scale is expectedly of the order of 15% of the FSR in the range between 1500 and 1600 nm. In the visible region where stronger frequency dependences exist this will be expectedly worse.

In comparison to IBBCEAS the main advantages of DC-Coin are: (a) the significantly higher spectral resolution, and (b) the elimination of equipment to spectrally select the wavelengths of the transmitted light (e.g. a monochromator/CCD assembly or Fourier transform spectrometer) [21]. This high resolution aspect is an inherent strength of DCS and has been exploited here for the first time in a cavity-enhanced absorption approach using an incoherent light source.

5. Conclusion

In this publication we showed how to combine incoherent broadband cavity enhanced absorption spectroscopy (IBBCEAS) with the principles of dual-comb spectroscopy (DCS) to yield an alternative approach to cavity-enhanced dual-comb spectroscopy. In "*Dual-Cavity Dual-Comb INterferometry (DC-COIN)*" incoherent light is passively coupled to two optically stable quasi-confocal cavities whose transmissions are combined and detected with a fast photodiode. The fast Fourier transform of the resulting interferogram yields a beat spectrum from which the absorption of a sample in the cavity can be retrieved. Depending on the cavities' geometries the method can exhibit high spectral resolution and good time resolution. Absolute wavenumbers can be determined straightforwardly by use of a single mode tunable diode laser or through a known absorption line in the reference or sample spectrum. In the current proof-of-concept work, spectra of H_2O, CO_2 and C_2H_2 were measured over ~2.6 cm^{-1} with a resolution of ~300 MHz in an integration time of 200 ms within the spectral region 1540–1560 nm using a spectrally filtered and amplified superluminescent light emitting diode. The 3σ noise equivalent absorption of the current dual-cavity setup (cavity length ~50 cm and R ~ 0.99978) was found to be 3.15×10^{-7} cm^{-1} $Hz^{-1/2}$. Improving the mechanical and temperature stability of the cavities would further improve this specific limit. The measurement concept can be expanded easily to different spectral regions including the mid IR provided an appropriate light source can be found. Other criteria for the applicability of this method have been discussed.

CRediT authorship contribution statement

Jarni Braal: Writing – review & editing, Validation, Software, Methodology, Investigation, Formal analysis, Data curation. **Satheesh Chandran:** Writing – review & editing, Validation, Supervision, Investigation. **Robert Sheehan:** Writing – review & editing, Validation, Resources, Investigation. **Anton J. Walsh:** Validation, Supervision, Resources, Methodology, Conceptualization. **Albert A. Ruth:** Writing – original draft, Visualization, Validation, Supervision, Resources, Project administration, Methodology, Funding acquisition, Conceptualization.

Funding

This work was supported through a Research Ireland's Frontiers for the Future Award (21/FFP-A/8973) and the Irish Research Council (GOIPG/2021/1263).

Declaration of competing interest

The authors declare that they have no known competing financial interests or personal relationships that could have appeared to influence the work reported in this paper.

Acknowledgments

J. Braal thanks the Irish Research Council for a governmental postgraduate fellowship. S. Chandran and A. Walsh were also supported

through Research Ireland's Pathway Programme (21/PATH-S/9430). The authors thank Steve DePuis for the construction of an enclosure for the optical setup, Prince Anandarajah for advice on building an appropriate light source, Frank Peters for the loan of an ECDL and other equipment, and Steve Hegarty for discussions on the data analysis.

Appendix A. Supplementary data

Supplementary data to this article can be found online at https://doi.org/10.1016/j.optlastec.2026.115393.

Data availability

Data underlying the results presented in this paper are available from the corresponding author upon request.

References

[1] S. Schiller, Spectrometry with frequency combs, Opt. Lett. 27 (2002) 766–768.
[2] F. Keilmann, C. Gohle, R. Holzwarth, Time-domain mid-infrared frequency-comb spectrometer, Opt. Lett. 29 (2004) 1542–1544.
[3] I. Coddington, W.C. Swann, N.R. Newbury, Coherent multiheterodyne spectroscopy using stabilized optical frequency combs, Phys. Rev. Lett. 100 (2008) 013902.
[4] I. Coddington, N. Newbury, W. Swann, Dual-comb spectroscopy, Optica 3 (2016) 414–426.
[5] S.A. Diddams, D.J. Jones, J. Ye, et al., Direct link between microwave and optical frequencies with a 300 THz Femtosecond Laser Comb, Phys. Rev. Lett. 84 (2000) 5102–5105.
[6] A. Schliesser, M. Brehm, F. Keilmann, et al., Frequency-comb infrared spectrometer for rapid, remote chemical sensing, Opt. Exp. 13 (2005) 9029–9038.
[7] G. Rieker, F. Giorgetta, W. Swann, et al., Frequency-comb-based remote sensing of greenhouse gases over kilometer air paths, Optica 1 (2014) 290–298.
[8] K.C. Cossel, E.M. Waxman, F.R. Giorgetta, et al., Open-path dual-comb spectroscopy to an airborne retroreflector, Optica 4 (2017) 724–728.
[9] K.C. Cossel, E.M. Waxman, E. Baumann, et al., Remote sensing using open-path dual-comb spectroscopy, in: W. Chen, D.S. Venables, M.W. Sigrist (Eds.), Advances in Spectroscopic Monitoring of the Atmosphere, Elsevier, Amsterdam, 2021, pp. 27–93.
[10] J.J. Han, W. Zhong, R.C. Zhao, et al., Dual-comb spectroscopy over a 100 km open-air path, Nat. Photon. 18 (2024) 1195–1202.
[11] A. Foltynowicz, P. Mas1owski, T. Ban, et al., Optical frequency comb spectroscopy, Faraday Discuss. 150 (2011) 23–31.
[12] P.L. Luo, Long-wave mid-infrared time-resolved dual-comb spectroscopy of short-lived intermediates, Opt. Lett. 45 (2020) 6791–6794.
[13] M.J. Thorpe, K.D. Moll, R.J. Jones, et al., Broadband cavity ringdown spectroscopy for sensitive and rapid molecular detection, Science 311 (2006) 1595–1599.
[14] B. Bernhardt, A. Ozawa, P. Jacquet, et al., Cavity-enhanced dual-comb spectroscopy, Nat. Photon. 4 (2010) 55–57.
[15] A.J. Fleisher, D.A. Long, Z.D. Reed, et al., Coherent cavity-enhanced dual-comb spectroscopy, Opt. Exp. 24 (2016) 10424–10434.
[16] N. Hoghooghi, R.J. Wright, A.S. Makowiecki, et al., Broadband coherent cavity-enhanced dual-comb spectroscopy, Optica 6 (2019) 28–33.
[17] T. Gherman, E. Eslami, D. Romanini, et al., High sensitivity broad-band mode-locked cavity-enhanced absorption spectroscopy: measurement of $Ar^*(^3P_2)$ atom and N_2^+ ion densities, J. Phys. D Appl. Phys. 37 (2004) 2408–2415.
[18] S. Chandran, A.A. Ruth, E.P. Martin, et al., Off-axis cavity-enhanced absorption spectroscopy of $^{14}NH_3$ in air using a gain-switched frequency comb at 1.514 μm, Sensors 19 (2019) 5217–5232.
[19] G. Guan, A. Liu, X. Wu, et al., Near-infrared off-axis cavity-enhanced optical frequency comb spectroscopy for CO_2/CO dual-gas detection assisted by machine learning, ACS Sens. 9 (2024) 820–829.
[20] D.W. Chandler, K.E. Strecker, Dual-etalon frequency-comb cavity ringdown spectrometer, J. Chem. Phys. 136 (2012) 154201.
[21] A.A. Ruth, S. Dixneuf, R. Raghunandan, "Broadband cavity-enhanced absorption Spectroscopy with incoherent light", in: "Cavity enhanced spectroscopy and sensing", Eds. G. Gagliardi and H.P. Loock, Springer Series in Optical Sciences, vol. **179**, 485–517 (2014).
[22] K.Y. Zheng, C.T. Zheng, Y. Zhang, et al., Review of incoherent broadband cavity-enhanced absorption spectroscopy (IBBCEAS) for gas sensing, Sensors 18 (2018) 3646.
[23] S.E. Fiedler, A. Hese, A.A. Ruth, Incoherent broad-band cavity-enhanced absorption spectroscopy, Chem. Phys. Lett. 371 (2003) 284–294.
[24] A.A. Ruth, J. Orphal, S.E. Fiedler, Cavity enhanced Fourier transform absorption spectroscopy using an incoherent broadband light source, Appl. Opt. 46 (2007) 3611–3616.
[25] J. Orphal, A.A. Ruth, High-resolution Fourier-transform cavity-enhanced absorption spectroscopy in the near-infrared using an incoherent broad-band light source, Opt. Express 16 (2008) 19232–19243.
[26] R.M. Varma, D.S. Venables, A.A. Ruth, et al., Long optical cavities for open-path monitoring of atmospheric trace gases and aerosol extinction, Appl. Opt. 48 (2009) B159–B171.
[27] M. Bitter, S.M. Ball, I.M. Povey, et al., A broadband cavity ringdown spectrometer for in-situ measurements of atmospheric trace gases, Atmos. Chem. Phys. 5 (2005) 2547–2560.
[28] W. Zhang, X. Chen, X. Wu, et al., Adaptive cavity-enhanced dual-comb spectroscopy, Photon. Res. 7 (2019) 883–889.
[29] D. Charczun, A. Nishiyama, G. Kowzan, et al., Dual-comb cavity-mode width and shift spectroscopy, Measurement 188 (2022) 110519.
[30] D. Lisak, D. Charczun, A. Nishiyama, et al., Dual-comb cavity ring-down spectroscopy, Sci. Rep. 12 (2022) 2377.
[31] C.C. Teng, J. Westberg, G. Wysocki, Gapless tuning of quantum cascade laser frequency combs with external cavity optical feedback, Opt. Lett. 48 (2023) 363–366.
[32] X. Ren, J. Pan, M. Yan, et al., Dual-comb optomechanical spectroscopy, Nature Comm. 14 (2023) 5037.
[33] B. Tang, W. Zhang, M. Lu, et al., Cavity-enhanced dual-comb spectroscopy with wide spectral band tuning, Appl. Phys. Lett. 124 (2024) 181110.
[34] H. Sun, D. Wen, K.-P. Cheong, et al., Cavity-enhanced dual-comb spectroscopy for sensitive OH detection in a laminar premixed flame, Proc. Combust. Inst. 41 (2024) 105662.
[35] H. Sun, M. Hu, Q. Nie, et al., Cavity-enhanced dual-comb spectroscopy stabilized by molecular absorption line locking, Appl. Phys. Lett. 125 (2024) 251103.
[36] C.R. Markus, J. Hayden, D.I. Herman, et al., Cavity-enhanced dual-comb spectroscopy in the molecular fingerprint region using free-running quantum cascade lasers, JOSA B 41 (2024) E56–E64.
[37] I.E. Gordon, L.S. Rothman, R.J. Hargreaves, et al., The HITRAN2020 molecular spectroscopic database, J. Quant. Spectrosc. Rad. Trans. 277 (2022) 107949.
[38] S.N. Mikhailenko, Y.L. Babikov, V.F. Golovko, Information-calculating system Spectroscopy of Atmospheric gases. The structure and main functions, Atmosph. Ocean. Opt. 18 (2005) 685–695.
[39] E.J. Moyer, D.S. Sayres, G.S. Engel, et al., Design considerations in high-sensitivity off-axis integrated cavity output spectroscopy, Appl. Phys. B 92 (2008) 467–474.
[40] P. Werle, R. Miicke, F. Slemr, The limits of signal averaging in atmospheric trace-gas monitoring by tunable diode-laser absorption spectroscopy (TDLAS), Appl. Phys. B 57 (1993) 131–139.
[41] A.E. Siegman, *Lasers*, University Science Books, Sausalito CA, 1986.
[42] D.I. Herman, M. Walsh, M.K. Kreider, et al., Squeezed dual-comb spectroscopy, Science 387 (2025) 653–658.
[43] Z. Wan, Y. Chen, X. Zhang, et al., Quantum correlation-enhanced dual-comb spectroscopy, Light Sci. Appl. 14 (2025) 257.
[44] A. Foltynowicz, T. Ban, P. Masłowski, et al., Quantum-noise-limited optical frequency comb spectroscopy, Phys. Rev. Lett. 107 (2011) 233002.
[45] L. Rutkowski, A.C. Johansson, G. Zhao, et al., Sensitive and broadband measurement of dispersion in a cavity using a Fourier transform spectrometer with kHz resolution, Opt. Exp. 25 (2017) 21711–21718.
[46] S. Boudreau, J. Genest, Referenced passive spectroscopy using dual frequency combs, Opt. Exp. 20 (2012) 7375–7387.
[47] L.A. Sterczewski, J. Westberg, G. Wysocki, Computational coherent averaging for free-running dual-comb spectroscopy, Opt. Exp. 27 (2019) 23875–23893.
[48] A. Eber, C. Gruber, M. Schultze, et al., Streaming self-corrected dual-comb spectrometer, Opt. Exp. 33 (2025) 35314–35325.
[49] Q. Liang, A. Bisht, A. Scheck, et al., Modulated ringdown comb interferometry for sensing of highly complex gases, Nature 638 (2025) 941–948.
[50] M.J. Thorpe, R.J. Jones, K.D. Moll, et al., Precise measurements of optical cavity dispersion and mirror coating properties via femtosecond combs, Opt. Exp. 13 (2005) 882–888.